# Properties of the Bulalo Geothermal Reservoir Top based on Core Analysis

J.A. STIMAC[1]
Chevron Geothermal Indonesia, Jakarta, Indonesia

[1]Chevron Geothermal Salak, Ltd., 11th Floor Sentral Senayan I, Jl. Asia Afrika No. 8, Jakarta, 10270, Indonesia
Ph. (62 21) 5798 4547 Fax (62 21) 573 0991

# PROPERTIES OF THE BULALO GEOTHERMAL RESERVOIR TOP BASED ON CORE ANALYSIS

J.A. STIMAC[1]

[1]Chevron Geothermal Salak, Ltd., 11th Floor Sentral Senayan I, Jl. Asia Afrika No. 8, Jakarta, 10270, Indonesia

**SUMMARY –** Core analysis integrated with other data indicates that the top of the Bulalo geothermal reservoir is a corrugated surface controlled by the first point of downward continuous open space in linked fractures that terminate upward in ductile clay-rich lithologies or are blocked by partially sealed veins. Fault-valve action likely mediated cycles of upward growth and resealing of such fracture systems at initial conditions. Declining fluid pressure and minimum stress influence the depth and integrity of the reservoir top seal once fluid production is underway. The presence of large fractures that are locally open, the declining minimum stress due to fluid production, and thermal affects associated with pumping cold fluid in a hot borehole all impact the ability of seal rocks near the reservoir top to maintain fluid pressure during leakoff tests (LOT). Considering these factors, LOT are of limited value in determining if well design criteria have been met. Plug porosity (4 to 14%) and permeability (<0.001 to 0.1 md) are typical of reservoir rocks, but permeability ranges to higher values (0.1 to 0.2 md) for samples that have well-oriented, partially filled fractures parallel to the plug axis. Horizontal plugs from the ash-flow tuff have higher permeability than vertical plugs from the same rock indicating welding and hydrothermal processes promote higher horizontal permeability. Porosity and vertical permeability of whole core is similar to that measured on plugs, but permeability measured in the horizontal plane ranges to higher values (4 to 9 md) due to sampling of larger more partially open fractures proximal to faults.

## 1. INTRODUCTION

The Bulalo geothermal field, now operated by Chevron Geothermal Philippines Holdings Company, Inc., is the second largest producer of geothermal energy in the Philippines (Stimac et al., 2006; Golla et al., 2001). Core was taken in well Bulalo-110 to better understand controls on the top of the reservoir and characterize the fracture and rock matrix properties at that depth.

The ultimate goal of the study was to improve our model of the Bulalo reservoir top and use this model to select the optimum depth of the cemented 13-3/8" casing for deep wells in terms of minimizing well cost and risk of well failure (Menzies et al., 2007). The core improved our understanding of leakoff tests (LOT) and, in particular, how existing fractures and thermal forces affect the results of LOT in the geothermal environment.

## 2. METHODS AND RESULTS

Several near-vertical fractures with evidence of offset (faults) are present in the cored interval. To fully characterize the orientations and flow properties of fractures, goniometry and re-orientation of the core by paleomagnetic methods was done. Paragenetic and fluid inclusion studies further constrained the history of fracture deformation and sealing.

We sampled six portions of the core (Fig. 1) for measurement of fractures, veins and rock matrix properties (compressional strength, density, sonic velocity, porosity, permeability, and thermal expansion). Four of these core segments are partially welded andesite ash-flow tuff. Two of these segments are of relatively unveined matrix rock (A and C, Fig. 1); the other two are of more intensely veined matrix adjacent to major faulted veins. These latter veined areas are between the main faulted vein and near-vertical subsidiary veins (O and J, Fig. 1). A fifth segment of tuff is relatively unveined, but contains large pumice that might influence its bulk matrix properties (M). The final segment of core is of the dense andesite lava. This lithology is homogeneous and unveined, so it has relatively constant matrix properties (Fig. 1).

### 2.1 Lithologic Description

The main core section from 2350.0 to 2361.17 ft (716.3 to 719.8 m) consists of partially-welded andesitic ash-flow tuff containing moderately flattened pumice (up to 5 cm) rich in chlorite and generally more porous than the bulk matrix (Fig. 1). The matrix contains <5% lithic fragments of basaltic to andesitic lava. The tuff did not undergo extensive primary devitrification, so its matrix contained a significant amount of glass subsequently converted mainly to chlorite, mixed layer clay, titanite, and quartz.

Dense porphyritic basaltic andesite lava lies below the tuff (assumed depth 2361.2 to 2361.7 ft or 719.7 to 719.8 m). It has a microcrystalline matrix with little or no interstitial glass and therefore was not very susceptible to hydrothermal alteration. It lacks fractures or veins (R in Fig. 1).

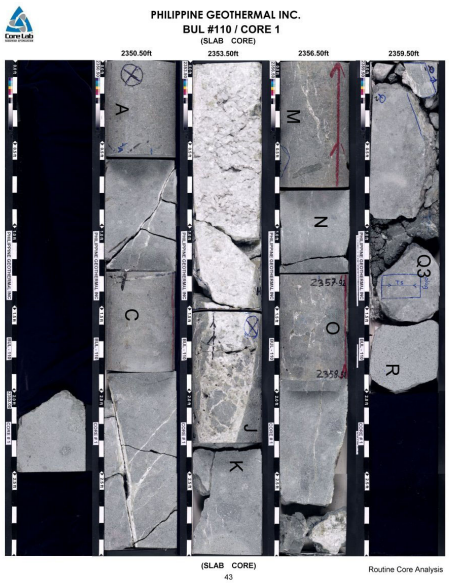


Figure 1. Photo of slabbed core. Andesite tuff (all core except segment R) and unveined basaltic andesite lava (lower right, labelled R). Unslabbed segments were used for whole-core porosity and permeability studies and rock mechanics. All natural fractures show some mineral filling.

### 2.2 Fault, Fracture and Vein Description

The andesite tuff is cut by 3 near-vertical faults partially filled with sheared veins (Fig. 1). Figure 2 shows an idealized distribution of the major and minor fractures and breccias observed. These partially-open fractures strike NW and dip 53-80 degrees. Maximum apertures range from 5 to 15 mm, but average 2 mm. The fractures exhibit clear evidence of offset, with a dip-slip sense of movement. This is shown by abraded crystal surfaces along points of contact and grooving along the dip direction of the fracture. There is also evidence for offset of pumice fragments along the fracture walls, with a normal sense of displacement. Some calcite-cemented breccias and crushed zones are localized along the major fractures, especially along slight bends (e.g., segment J in Fig. 1).

Several types of subsidiary fractures are associated with the faults. One set formed at 30 to 60 degrees to the main fault plane (Fig. 2), suggesting they are conjugate fractures to the main structure. They commonly originate along the main fault, but in some cases continue across it with no apparent offset. In one case there is evidence of minor offset on these features on one side of the major vein. Very thin (0.1 mm) near-horizontal fractures are present and some show small (mm-scale) offset of near-vertical/conjugate fractures.

Most of these conjugate fractures have been partially filled with secondary minerals, but in thin section it can be seen that some open-space still exists along them. Subsidiary veins have maximum dimensions (kinematic aperture or filled width) up to 5 mm near their intersections with the major fracture, but are generally <2 mm away from the intersection. Many subparallel conjugate veins with widths <1 mm are present near the faults, but terminate within a few centimeters.

Near-vertical fractures extend from the main fractures in both the hanging wall and footwall, and are occasionally associated with the jigsaw puzzle breccias mentioned above. These fractures mainly are filled with secondary minerals. They have maximum dimensions of several mm (average about 1 mm thick) and tend to be more variable in orientation, with horsetails and wispy terminations.

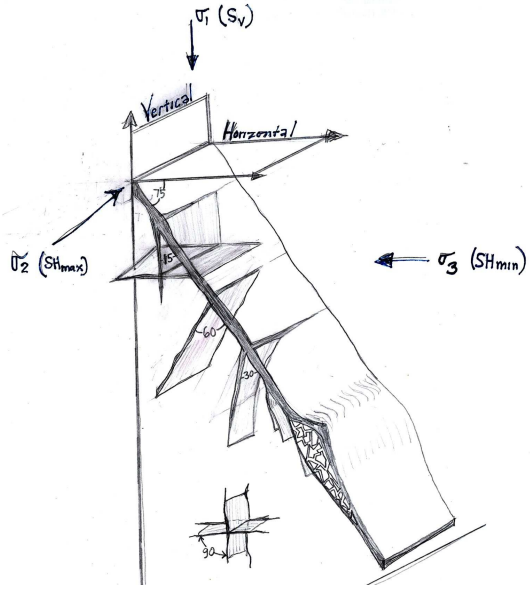


Figure 2. Summary of major fracture and breccia types found in the Bul-110 core. The geometry of large open fractures and subsidiary minor fractures is consistent with all having formed in multiple episodes of normal faulting, possibly facilitated by fluid overpressure.

In summary, the series of minor normal faults and subsidiary fractures at the top of the Bulalo reservoir (Fig. 2) is similar to a basic model for a normal fault formed in a stress field with a vertical principle stress presented by Caine and Forster (1999). Such fractures form perpendicular to the $SH_{min}$, and typically strike along the direction of $SH_{max}$.

### 2.3 Orientation of Fractures

A Master Orientation Line (MOL) was drawn on the core to provide a directional reference. The dips and azimuths of 41 fractures were measured relative to the MOL with a PG200 Portable Goniometer linked to a computer at CoreLab (Jakarta). The true orientation of the MOL was then determined by paleomagnetism and the dip azimuth data rotated accordingly by Core Magnetics, UK (CoreLab, 2004).

The goal of the paleomagnetic study was to determine the line of true north in the samples and thereby correct the goniometry reading to its true azimuth. This required measurement of the characteristic remnant magnetization of several paired plug samples taken over the length of the core. Strong, stable, and consistent natural remnant magnetizations were observed in all plug pairs with slight deviation of the 2 deepest plugs, probably due to errors marking the MOL.

Paleomagnetically-corrected fracture dips are summarized in Figure 3. It can be seen that steeply-dipping fractures predominate. More than 70% of the fracture population and all faults dip >50 degrees. The abundance of fractures in the >50 to <70 degree range is consistent with a normal faulting regime, whereas the abundance of near-vertical fractures may be related to hydraulic opening (e.g., Caine and Forster, 1999).

The three faults with multiple episodes of movement have strike azimuths of 149°, 133°, and 102° and dips of 53°, 77°, and 80°, respectively. Most faults at Bulalo have either NE or NW strikes.

### 2.4 Vein Mineral Assemblages and Paragenesis

Vein assemblages were examined in thin sections to determine the minerals present and their parageneses. The major open fractures in the core represent small-displacement faults with multiple episodes of movement. Two to three distinct episodes of mineral precipitation can be identified in most faulted veins, indicating episodes of reopening and shear deformation. Petrography also confirms brecciation on a very fine scale with later overgrowths of crack-seal textured minerals (Fig. 4).

The following paragenetic sequence can be inferred from sheared veins (Figs. 4 and 5):

1. Initial Faulting → Acicular epidote (± Calcite)
2. Quartz → Local fault re-opening → Quartz (± Prehnite ± Adularia)
3. Local fault re-opening (± xl frags) → Calcite
4. Dissolution of Calcite → Feathery Chlorite

This paragenesis suggests that hot, overpressured hydrothermal fluids ascended to the reservoir top during an episode of fault rupture, and that epidote ± calcite was rapidly precipitated. It appears many of the subsidiary fractures were also formed at this time, since they are dominated by epidote ± calcite, but commonly lack quartz ± prehnite. The needle-like crystal form of epidote suggests rapid growth, either due to boiling or cooling of the fluid (Fig. 5). The presence of early calcite with epidote in some subsidiary veins is consistent with boiling, but no bladed calcite is present that would imply vapor-dominated conditions. Most major veins show evidence for early growth of acicular epidote, followed by quartz and prehnite, followed by coarse-grained blocky calcite (Figs. 4, 5). A few samples show corrosion of late calcite and deposition of feathery chlorite.

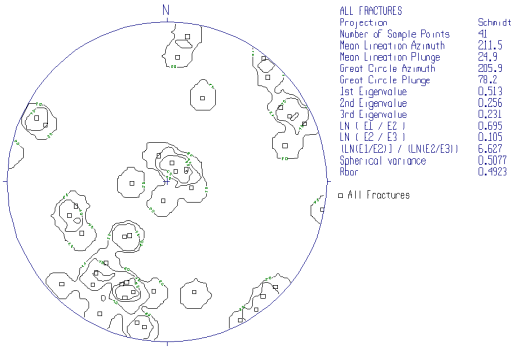


Figure 3. Stereonet of dip azimuths of fractures (n=41).

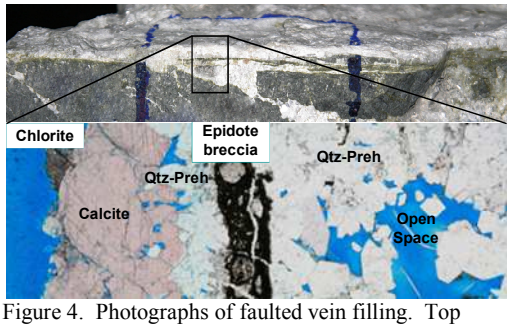


Figure 4. Photographs of faulted vein filling. Top photo shows quartz-prehnite that has encapsulated mylonitic epidote-rich breccia lenses (green layers). The black box shows the area of transect in the bottom photo. Vein filling sequence is sheared epidote (middle), encapsulated by quartz-prehnite (right), followed by blocky calcite (later corroded, stained pink) overgrown by minor feathery chlorite left).

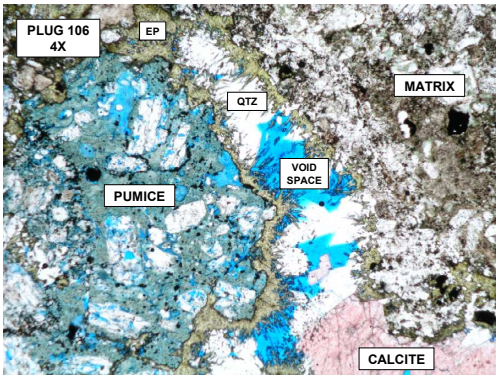


Figure 5. Subsidiary vein with early acicular epidote, later quartz, and latest blocky calcite near its intersection with the major vein (bottom of photo). Blue dye shows open space remains within the vein and adjacent chloritized pumice in the tuff matrix.

Mineral fillings in faults show complex textures including mylonitic layers rich in epidote, fragments of quartz and epidote sandwiched between euhedral quartz and blocky calcite.

These features indicate a second episode of vein opening that sheared early epidote.

Other veins show evidence for a similar episode of shearing, based on the occurrence of finely broken quartz and epidote debris present in pockets formed by euhedral quartz, followed by massive growth of calcite. The irregular growth forms of quartz crystals suggest that they grew during rapid boiling, consistent with re-opening of the fault (Joe Moore, personal communication, 2004). The blocky calcite that dominates most large veins is euhedral where open space remained, but locally filled the vein and was subsequently broken or badly sheared or abraded. In some cases calcite shows evidence of dissolution, and feathery overgrowths of chlorite were deposited locally.

Fluid inclusion temperatures were reported for a variety of Bulalo vein samples by Stimac et al. (2006). Homogenization temperatures and salinities of inclusions in quartz and calcite from Bul-110 veins range up to 279ºC and 1.05 wt% $NaCl_{eq}$, respectively. Inclusions with lower temperatures (260-213ºC) and salinities (0.6 to 0.0 wt% $NaCl_{eq}$) reflect dilution by steam-heated waters and steam condensate. Influx of relatively cool steam heated waters may have occurred due to upward fracturing and faulting. Subsequent resealing of fractures has apparently led to re-establishment of the higher temperatures measured in the well.

### 2.5 Porosity and Permeability

Plug and whole-core measurements of porosity and permeability reveal that horizontal permeability is higher than vertical permeability and subsidiary fractures play a significant role in enhancing fluid flow in the vicinity of faults (Figs. 6, 7 and Tables 1, 2).

Plug permeability is typical of that found in reservoir rocks (0.001 to 0.2 md). The highest values are for samples that have well-oriented, partially filled fractures parallel to the plug axis (0.1 to 0.2 md). Horizontal plugs from the tuff have higher permeability than vertical plugs indicating that welding, angled fractures, and/or hydrothermal processes promote higher horizontal permeability. Whole-core also has higher horizontal than vertical permeability, but horizontal permeability ranges to higher values (4 to 9 md) because larger partially-open fractures near faults were more fully sampled (Fig. 8).

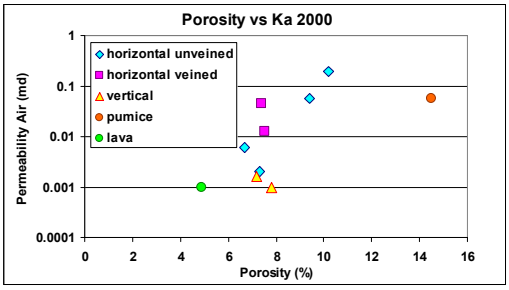


Figure 6. Plug porosity versus Ka measured at 2000 psi net stress. Permeability to air = Ka.

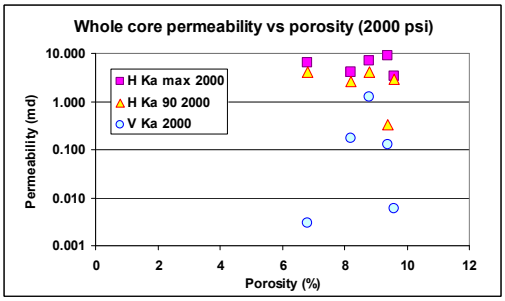


Figure 7. Whole-core Ka as a function of orientation of the flow path at 2000 psi. H=horizontal; V=vertical.

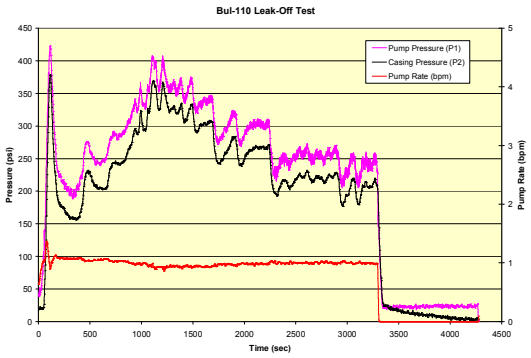


Figure 8. Bul-110 Leak-off test pressure versus time.

### 2.6 Compressional Strength and Thermal Expansion

Triaxial strength tests and coefficient of thermal expansion measurements (Table 3) were made on the tuff and lava samples. The andesite lava has a higher unconfined compressive strength (UCS =158.6 MPa or 23,000 psi) and thermal expansion coefficient (by almost a factor of 2) than the tuff (UCS= 65.5 to 113.8 MPa or 9,500 to 16,500 psi). The results suggest that compact crystalline rocks like the andesite lava, while strong, may be more susceptible to thermal fracturing than more ductile tuffaceous rocks.

Table 1. Whole core data.

| | Sample | Depth | | Horizontal Perm | | Vertical Perm | Porosity | Grain Density | Remarks |
|---|---|---|---|---|---|---|---|---|---|
| | | Top | Bottom | Kair (Max) | Kair (90°) | Kair (Vert.) | | | |
| | | (Feet) | (Feet) | (md) | (md) | (md) | (%) | (gm/cc) | |
| **A** | **FD 1** | 2350.50 | 2351.08 | 6.90 | 4.07 | 1.260 | 8.5 | 2.67 | single fracture |
| **C** | **FD 2** | 2351.75 | 2352.30 | 6.34 | 4.10 | 0.003 | 6.5 | 2.67 | single fracture |
| **J** | **FD 3** | 2355.00 | 2355.84 | 9.06 | 0.33 | 0.130 | 9.1 | 2.69 | stockwork fractured, vuggy |
| **M** | **FD 4** | 2356.50 | 2357.25 | 3.30 | 2.93 | 0.006 | 8.7 | 2.69 | vuggy |
| **O** | **FD 5** | 2357.92 | 2358.50 | 4.08 | 2.66 | 0.170 | 6.4 | 2.67 | ribbony fractures |

Letters in first column refer to core segment (see Figs. 1 and 2). FD= full diameter.
Andesite ash-flow tuff, 2000 psi confining pressure

Table 2. Plug data.

| | Sample | Depth | Perm Kair | Porosity | Grain Density | Remarks | Thin Section Description of Perm |
|---|---|---|---|---|---|---|---|
| | | (ft) | (md) | (%) | g/cm3 | | |
| **A** | 101 | 2351.58 | 0.0555 | 9.4 | 2.69 | from FD1 | Intact sample, minor thin veins. Highest optical perm: blue dye along microchannels and cc-qtz-py veins, dissolution in pyx & plag, and pumice |
| **C** | 102 | 2351.88 | 0.197 | 10.2 | 2.70 | from FD2 | |
| **J** | 106 | 2355.16 | 0.0441 | 7.4 | 2.72 | veined zone from FD3 | Lots of cc breccia filling/veining. Large voids in vuggy fillings, some minor fractures. Almost all blue dye along fractures. |
| **K** | 107H | 2356.25 | 0.006 | 6.7 | 2.71 | horizontal plug | Vertical and horizontal plugs through similar rock |
| **K** | 107V | 2356.00 | 0.0016 | 7.2 | 2.70 | vertical plug | |
| **M** | 107A | 2357.08 | 0.0571 | 14.5 | 2.72 | angled plug; pumice from FD4 | |
| **N** | 108V | 2357.58 | 0.001 | 7.8 | 2.70 | | Blue dye in vertical ep-cc-qtz vein, pumice, and matrix channelways. |
| **O** | 109 | 2357.97 | 0.0126 | 7.5 | 2.71 | veined zone from FD5 | Moderate blue dye along cc veins and py-ep-cc veins and nearby matrix. |
| **Q3** | 111 | 2360.92 | 0.0020 | 7.3 | 2.74 | | |
| **R** | 112V | 2361.33 | 0.0010 | 4.9 | 2.81 | WC not done since sample homogeneous | Very minor blue dye in cracked/altered pyx, rare channelways. |

Letters in first column refer to core segment (see Figs. 1 and 2). FD= full diameter.
All samples andesite tuff except R, which is andesite lava

Table 3. Coefficient of Thermal Expansion values for the andesite lava and andesite ash-flow tuff **($10^{-6}$/°F).**

| Sample | Depth (ft) | $\alpha_{axial}$ 96 - 176°F | $\alpha_{axial}$ 176 - 266°F | $\alpha_{axial}$ 266 - 348°F | Avg over range | $\alpha_{volumetric}$ 96 - 176°F | $\alpha_{volumetric}$ 176 - 266°F | $\alpha_{volumetric}$ 266 - 348°F | Avg over range |
|---|---|---|---|---|---|---|---|---|---|
| Andesite Tuff | 2350.8 | 3.254 | 5.768 | 6.121 | 5.048 | 8.430 | 10.732 | 9.539 | 9.567 |
| Andesite Lava | 2360.25 | 6.586 | 9.776 | 10.880 | 9.081 | 11.876 | - | 16.170 | 14.023 |

## 2.7 Leak-off Test (LOT) Results

A LOT was conducted at 2420 ft (738 m) at a location where only minor fluid losses had been experienced while drilling (i.e., above the commercial reservoir top). A constant pump rate of 1 bpm was applied for 30 min, then pumps were turned-off to observe pressure fall-off. The 10 s shut-in pressure was used to calculate the fracture gradient at the shoe. Figure 8 shows that the LOT profile has a "saw-tooth" shape. The 10 s shut-in pressure was 1944 kPa (282 psi) and the computed fracture gradient was 12.67 kPa/m (0.56 psi/foot). This value is lower than the desired fracture gradient to drill to >3000 m (10,000 ft) at Bulalo (Menzies et al., 2007).

## 3. DISCUSSION

The tuff is moderately welded fragmental rock that was originally composed of glassy pyroclasts, whereas the lava was originally an intact, compact crystalline rock. The tuff consists of ash, pumice, crystals, and lithics that have different properties and impart more variability at the scale of the plug than does the lava.

The glassy fragmental rock was more extensively altered to chlorite and mixed-layer clay, among other minerals. Chlorite and clay are relatively weak minerals, easily subject to shear along their dominant cleavages. In addition, this rock contains more voids and partially-filled fractures than the lava. All these characteristics lead to a rock that is relatively ductile, low-density, and weak compared to the lava, which has lower porosity and is composed of interlocking matrix minerals that make the rock stronger and more brittle.

A study of thermal effects (Santarelli, 2004) concluded that they play a significant role in geothermal LOT, but no simple correction factor can be made to account for these effects. It has been estimated that a temperature changes are 300°F would create stress changes in the order of 69 MPa (10,000 psi). Since the tensile strength of the rock is about 10-20% of the compressive strength, tensile fracturing could easily occur due

to temperature changes, accounting for the "saw-tooth" profile of declining pressure observed during the LOT (Fig. 8). In detail the "saw-tooth" profile was attributed to fracture growth ahead of the fracturing fluid followed by slow fracture invasion and pressurization.

Reopening of partially sealed faults and fractures forming weak links in the rock provides another explanation for the "saw-tooth" pressure response. The occurrence of major, partially open fractures in the cored interval strongly supports this idea. While it would be expected that fractures propagated by the LOT will be perpendicular to the minimum *in situ* stress, they may also follow the orientation of existing, partially open fractures. Moreover, existing fractures provide more rapid and extensive access to the rockmass than would be achieved if the fractures were not present, facilitating thermal fracturing and resulting in more extensive loss of fluid.

LOT conducted near the top of geothermal reservoirs entail pumping cold fluid (<150˚F) into a relatively hot formation (>400˚F). Conversely, production of deep geothermal fluids would not cause the same thermal contraction as the cold fluid, and therefore LOT results are not easily interpreted in the geothermal setting. A LOT conducted with cold water would yield a lower fracture gradient; therefore, some method of correcting the LOT-derived fracture gradient for thermal effects is needed to correctly apply the fracture gradient data to well design criteria.

Core analysis integrated with other data indicates that the top of the Bulalo geothermal reservoir is a corrugated surface controlled by episodic growth and resealing of faults and subsidiary fractures. Sibson (1990, 1996) described the earthquake cycle and the formation fault-fracture meshes through hydrothermal fluid pressures fluctuations. He noted that fault-fracture systems subject to normally-pressured or slightly overpressured regimes are weak and prone to tensile failure in extensional settings. The core observations and LOT results presented here verify that fault-valve action likely mediated cycles of upward growth and resealing of such fracture systems at Bulalo.

## 4. CONCLUSIONS

The characteristics of normal faults and associated fractures indicate that episodic fracture growth and resealing control the top of the Bulalo reservoir. Porosity and permeability of the rock matrix is locally enhanced adjacent to faults due to only partial sealing of subsidiary fractures and breccias.

The compressive strength of rocks sampled near the top of the reservoir is high, but the integrity of the rockmass is compromised by the presence of locally-open fractures. Thermal effects make brittle lithologies with large thermal expansion coefficients susceptible to tensile failure. The "saw-tooth" shape of the LOT pressure response suggests that there was opening of new tensile fractures or reopening of weakly-cemented existing fractures enhanced by thermal effects.

## ACKNOWLEDGMENTS

Thanks to Frederic Santarelli (Geomec), Richard Studd (CoreLab), Wes Martin (TerraTek), Joe Moore (EGI), and Baldeo Singh and Tony Dimabuyu (both formerly of Unocal) for assistance with aspects of data gathering and interpretation. The permission of Chevron to publish this work is greatly appreciated.

## 5. REFERENCES

Caine, J.S., and Forster, C.B., 1999, Fault zone architecture and fluid flow: insights from field data and numerical modeling. In *Faults and Subsurface Fluid Flow,* Haneberg, W.C., Mozley, P.S., Moore, J.C., and Goodwin, L.B. (Eds), AGU Geophysical Monograph 113, pp. 101-127.

CoreLab, 2004, *Routine core analysis, fracture study, bulk and clay X-ray diffraction for PGI well 110*. Unpublished CoreLab report.

Golla, G.U., Abrigo, F., Alarcon, B.O., Molling, P.A., and Stimac, J., 2001, The Bulalo geothermal field, Philippines: Conceptual model of a prolific geothermal system. Proceedings 22nd PNOC-EDC Conference, p. 123-132.

Menzies, A.J., Swanson, R.J., and Stimac, J.A., 2007, Design issues for deep geothermal wells in the Bulalo geothermal field, Philippines. Geothermal Resource Council Transactions, Vol. 31, 251-256.

Santarelli, F.J., 2004, *Quantification of thermal effect of fracturing with cold water in the Bulalo and Salak geothermal fields*: Unpublished Geomec Report.

Sibson, R.H., 1990, Conditions of fault-valve behavior, In *Deformation Mechanisms, Rheology and Tectonics,* R.J. Knipe and E.H. Rutter (Eds.), Geol. Soc. Spec. Publ. 54, pp. 15-28.

Sibson, R.H., 1996, Structural permeability of fluid-driven fault-fracture meshes. *Jnl. Structural Geol.*, Vol. 18(8), 1031-1042.

Stimac, J., Moore, J., and Latayan, J., 2006, Hydrothermal alteration and evolution of the Bulalo Geothermal Field, Philippines, Geothermal Resource Council Transactions, Vol. 30, p. 959-964.

TerraTek, 2005, *Quasi-static, dynamic and thermal properties of selected cores from Bul-110 well, Philippines*: Unpublished TerraTek Report.